Optics and Lasers in Engineering 152 (2022) 106946

Contents lists available at ScienceDirect

Optics and Lasers in Engineering

journal homepage: www.elsevier.com/locate/optlaseng

Evaluation local strain of twisted bilayer graphene via moiré pattern

Yuan Hou [a,b], Shuai Zhang [c,d], Qunyang Li [c,d], Luqi Liu [a,*], Xiaoping Wu [b], Zhong Zhang [a,b,*]

[a] CAS Key Laboratory of Nanosystem and Hierarchical Fabrication, CAS Center for Excellence in Nanoscience, National Center for Nanoscience and Technology, Beijing 100190, China
[b] CAS Key Laboratory of Mechanical Behavior and Design of Materials, Department of Modern Mechanics, University of Science and Technology of China, Hefei 230027, China
[c] Applied Mechanics Laboratory, Department of Engineering Mechanics, and Center for Nano and Micro Mechanics, Tsinghua University, Beijing 100084, China
[d] State Key Laboratory of Tribology, Tsinghua University, Beijing 100084, China

ARTICLE INFO

Keywords:
Twisted bilayer graphene
Moiré pattern
Local strain
Bubble test

ABSTRACT

Twisted bilayer graphene with hexagonal moiré patterns have shown a variety of unusual physical and mechanical phenomena. Unfortunately, some residual strain is introduced during the fabrication process of twisted bilayer graphene, leading to the deformation of moiré pattern. In this work, we employed water assisted transfer approach to build the suspended twisted bilayer graphene over the microscale holes patterned SiO_2/Si substrate. Atomic force microscopy is involved to characterize the moiré pattern. Based on reciprocal vectors analysis, a theoretical model was proposed to extract the local strain of twisted bilayer graphene sample. The local strain of twisted bilayer graphene induced by the transfer process as well as the biaxial tensile stretch was evaluated respectively.

1. Introduction

Through stacking two monolayer graphenes with a twist angle, twisted bilayer graphene (tBLG) with hexagonal moiré pattern is built, which has resulted in a succession of spectacular scientific discoveries, such as superconductivity [1,2] and superlubricity [3–5] etc. However, graphene is prone to distortion because of the atomic thickness, which makes it easy to restore local residual strain during the preparation and application of tBLG [6]. Earlier works have proven that the local residual strain have a significant impact on the optical, electrical, and mechanical characteristics of tBLG [7–9]. Thus, it is critically important to characterize and evaluate local strain of the tBLG sample.

Traditional moiré patterns are created by overlaying periodic grids that have open and solid parts, with the solid sections being lines, dots, or other geometrical shapes [10–12]. When two sets of grids are superposed at a modest angle, a minor displacement of one grid can cause a substantial deformation of the components in a moiré pattern [13]. Such a principle can be attributed to the amplification effect of the moiré pattern for grid displacement [14,15], which has far-reaching implications in many fields such as experimental mechanics [11,16], optical engineering [17–19], and physics including strain analysis [20,21], defect analysis [22,23], and strain engineering [9,24]. Although the moiré pattern has been successfully used as an effective tool for strain analysis at the macro and micro scales, strain analysis at the nanoscale remains a challenge due to grid size limitations [25]. Inspiringly, graphene moiré pattern can be utilized to examine minuscule strain fields in tBLG with the help of scanning probe microscopy (AFM) [26–29] or transmission electron microscopy (TEM) [30].

Extensive studies of moiré patterns on tBLG have been done during the last ten years [31–35]. Miller et al. investigated the effect of uniaxial strain on the lengths of the moiré pattern to estimate the strain of the graphene lattice [36]. Wang et al. devised the hexagonal digital moiré method for three-dimensional structural characterization of hexagonal packed nanostructures by analyzing three groups of parallel moiré patterns [37]. Cosma et al. investigated the geometrical features of moiré patterns characteristic of a pair of two incommensurate misaligned crystals in graphene heterostructures with hexagonal lattice [38]. Marton et al. described the strain field of graphene via three variables including uniaxial strain, strain direction and interlayer twist angle, and solved the strain field based on the lengths of moiré patterns [7]. Wang et al. also conducted the strain analysis of twisted trilayer graphene [39]. To date, however, there is still less quantitative evaluation of local residual strain of tBLG via the moiré pattern. In this paper, we fabricate the suspended tBLG and use AFM to characterize the deformed moiré patterns. A theoretical model was used to analyze the local strain of tBLG via the change in terms of lengths of moiré pattern.

1.1. Theoretical model

The schematics of the moiré pattern created by twisted bilayer graphene are shown in Fig. 1(a). When two monolayer graphene sheets are layered with a twist angle, the upper and bottom graphene lattices

* Corresponding authors.
E-mail addresses: liulq@nanoctr.cn (L. Liu), zhong.zhang@nanoctr.cn (Z. Zhang).

https://doi.org/10.1016/j.optlaseng.2022.106946
Received 24 August 2021; Received in revised form 29 December 2021; Accepted 1 January 2022
Available online 20 January 2022

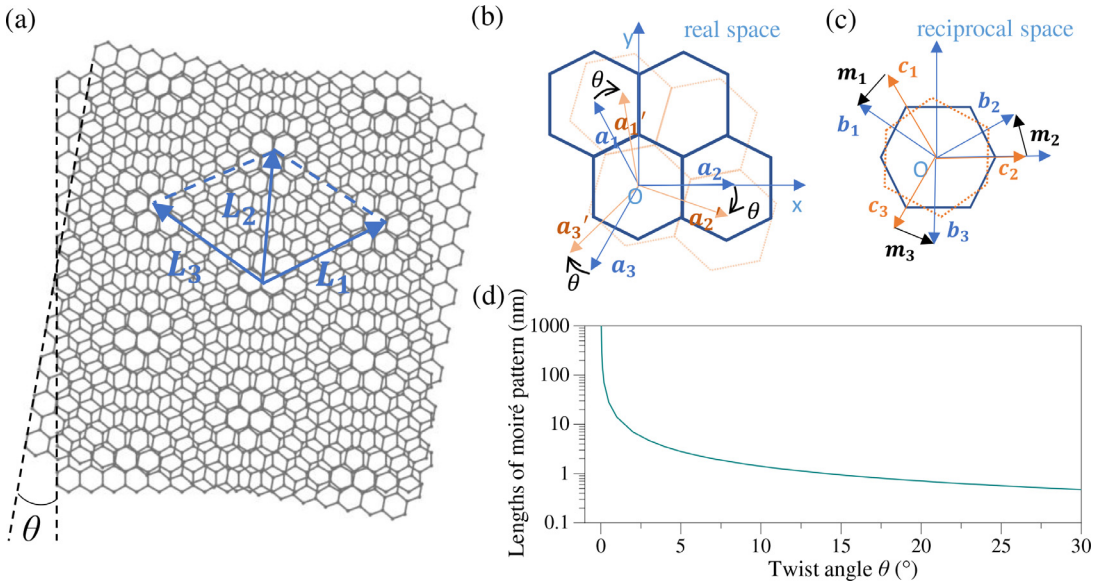

Fig. 1. (a) Schematics of moiré pattern of twisted bilayer graphene (tBLG), the rhombuses denote the moiré pattern unit cells. (b) graphene lattice vectors of tBLG. (c) reciprocal vectors of tBLG. (d) The relationship between the lengths of moiré pattern and twist angles of tBLG.

form two hexagonal grids, resulting in the hexagonal moiré pattern [40,41], which contains an alternating pattern of light and shade regions. The distances between consecutive light patches are represented by the lengths of the moiré pattern [L_1, L_2, L_3 in Fig. 1(a)]. Previous studies have shown that the lengths of moiré pattern are affected not only by the twist angle but also by the strain [6]. We begin our analysis with the graphene lattice vectors to determine the relationship between the lengths of the moiré pattern, twist angle, and strain field.

As illustrated in Fig. 1(b), the lattice vectors of the top graphene are defined as $\boldsymbol{a}_1$, $\boldsymbol{a}_2, \boldsymbol{a}_3$, while that of the bottom graphene as $\boldsymbol{a}_1', \boldsymbol{a}_2', \boldsymbol{a}_3'$. Then the reciprocal vectors of the top and bottom graphene are labeled as $\boldsymbol{b}_1$, $\boldsymbol{b}_2, \boldsymbol{b}_3$ and $\boldsymbol{c}_1$, $\boldsymbol{c}_2, \boldsymbol{c}_3$ respectively. The reciprocal vectors of the unstrained graphene are shown in Fig. 1(c), which can be written as [7],

$$\boldsymbol{b_i} = \begin{pmatrix} \cos\frac{(i-1)\pi}{3} \\ \sin\frac{(i-1)\pi}{3} \end{pmatrix} b, \quad b = \frac{4\pi}{\sqrt{3}a}, \quad i = 1, 2, 3 \tag{1}$$

The twist angle between the lower graphene and the upper graphene is θ, and the reciprocal vectors of the lower graphene are,

$$\boldsymbol{c_i} = \boldsymbol{R}(\theta)\boldsymbol{b_i} \tag{2}$$

$$\boldsymbol{R}(\theta) = \begin{pmatrix} \cos\theta & -\sin\theta \\ \sin\theta & \cos\theta \end{pmatrix} \tag{3}$$

Herein, the reciprocal vectors of graphene moiré pattern are,

$$\boldsymbol{m_i} = \boldsymbol{b_i} - \boldsymbol{c_i} \tag{4}$$

The lengths of the moiré pattern can be represented using the reciprocal vector transformation formula as,

$$L_i = \frac{4\pi}{\sqrt{3}|\boldsymbol{m_i}|} \tag{5}$$

When tBLG is strain-free condition, the preceding equation can be reduced to $L = a/2\sin(\theta/2)$. The relationship between twist angle and moiré pattern is then depicted in Fig. 1(d), where the length of the moiré pattern decreases as the twist angle increases.

Once the strain is applied to tBLG, two types of strain states are available. (i) The state of two layers of graphene subjected to separate strain fields [Fig. 2(a)] [42,43]. (ii) The same strain fields are applied to the top and bottom graphene, as seen in Fig. 2(b) [8,42].

i) In Fig. 2(a), the direction and value of strain should be considered for the residual strain of tBLG. The residual strain imparted on graphene's reciprocal vectors can be written as,

$$\boldsymbol{\xi}(\epsilon) = \begin{pmatrix} \frac{1}{1+\epsilon_1} & 0 \\ 0 & \frac{1}{1+\epsilon_2} \end{pmatrix} \tag{6}$$

The strain tensor can be further written as,

$$\boldsymbol{F}(\epsilon, \alpha) = \boldsymbol{R}^T(\alpha)\boldsymbol{\xi}(\epsilon)\boldsymbol{R}(\alpha) \tag{7}$$

$$\boldsymbol{R}(\alpha) = \begin{pmatrix} \cos\alpha & -\sin\alpha \\ \sin\alpha & \cos\alpha \end{pmatrix} \tag{8}$$

where α is the angle between the first principal strain ϵ_1 and the first reciprocal vector $\boldsymbol{b}_1$. Then the reciprocal vectors of graphene with residual strain could be expressed as,

$$\boldsymbol{b_i'} = \boldsymbol{F}(\epsilon, \alpha)\boldsymbol{b_i} \tag{9}$$

Herein, the reciprocal vectors of graphene moiré pattern are,

$$\boldsymbol{m_i} = \boldsymbol{b_i'} - \boldsymbol{c_i} \tag{10}$$

We can obtain the equations with three unknown variables $\epsilon_1, \epsilon_2, \alpha$ and three known variables L_1, L_2, L_3 by inserting Eqs. (6) (10) into Eq. (5). As a result, numerical solutions of Eq. (5) can be used to compute the strain field. The following are the steps in the calculation: i. Measure the lengths of the moiré pattern in three directions; ii. Compute the twist angle using a uniform moiré pattern; iii. Replace the measured parameters into Eq. (5); iv. Solve equations to map the local strain.

ii) In Fig. 2(b), both the top and bottom layer of tBLG is stretched together, so deformation of moiré pattern is compatible with graphene lattice deformation. The strain of the moiré pattern $\boldsymbol{\epsilon_m}$ can be used to predict the strain of the graphene lattice $\boldsymbol{\epsilon_l}$,

$$\boldsymbol{\epsilon_l} = \boldsymbol{\epsilon_m} = \frac{L_s - L_i}{Li} \tag{11}$$

where L_s and L_i denote the lengths of moiré patterns with and without strain. We can get the strain fields by measuring the lengths of the moiré pattern in three directions with the fixed initial twist angle.

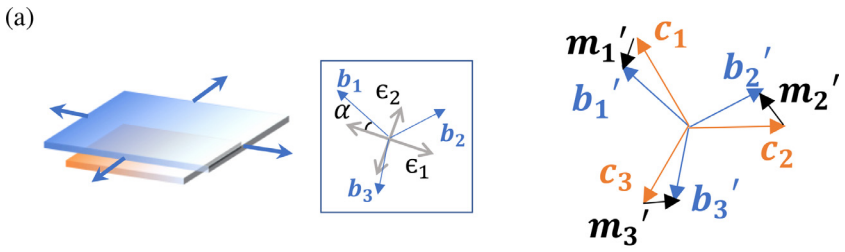

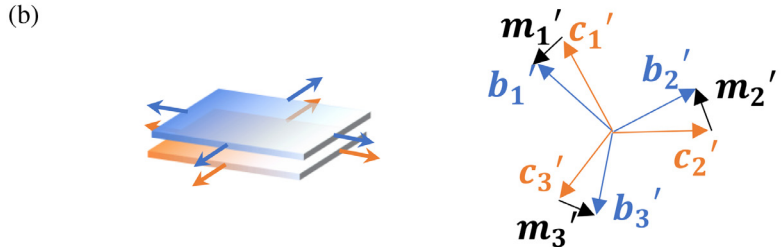

Fig. 2. (a) Schematics of the strain applied to the top layer of tBLG and the corresponding reciprocal vectors, where the strain direction is labeled in the square box. (b) Schematic of the same strain applied to the top and bottom layers of tBLG and the corresponding reciprocal vectors.

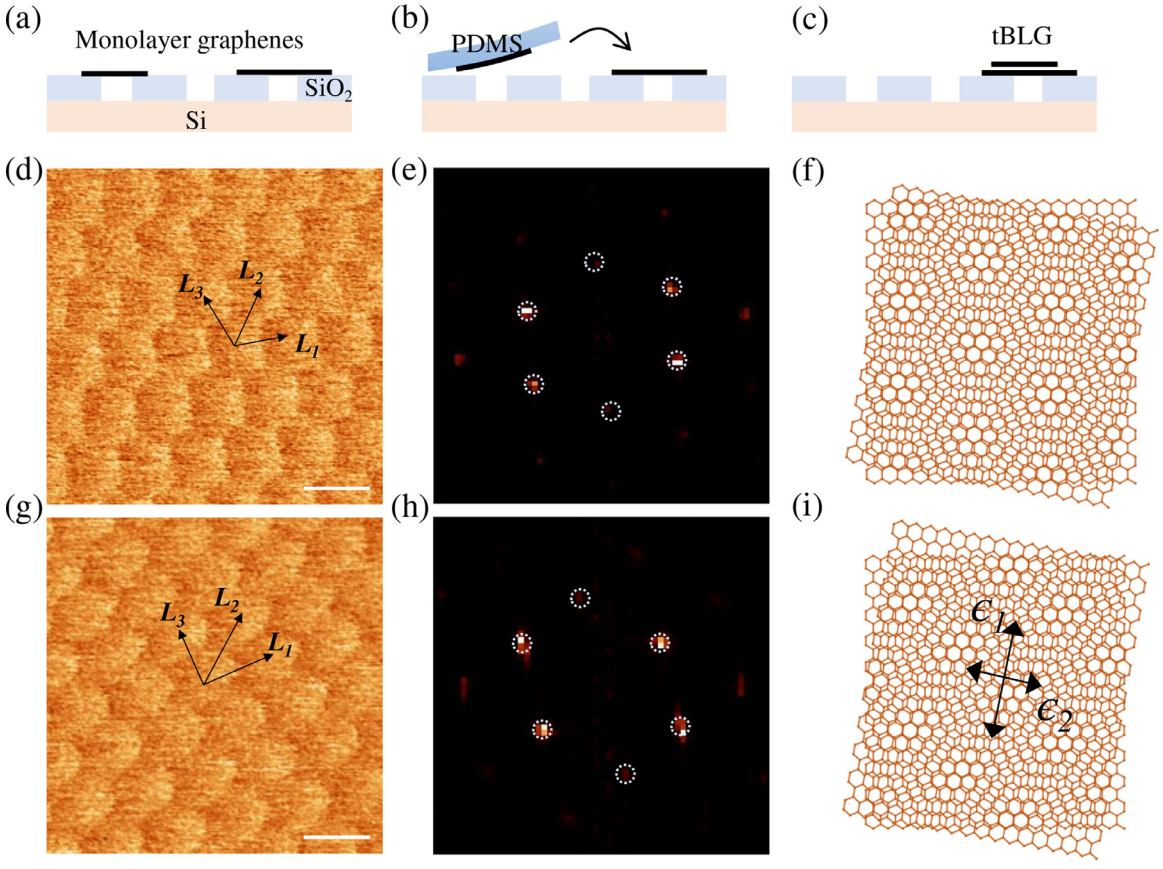

Fig. 3. (a-c) Schematics of the transfer process of tBLG. Lateral force images, diffraction patterns, and schematics of moiré pattern of tBLG with different local residual strains: (d-f) without strain; (g-i) with residual strain $\epsilon_1 \sim 0.31\%$, $\epsilon_2 \sim 0.01\%$. The black arrows in (d), (g) represent the vectors of moiré patterns of tBLGs. The arrows in (i) denote the directions of local residual strains of the top monolayer graphene. Scale bars: (d), (g) 20 nm.

1.2. Characterization of local residual strain induced by transfer process

Researchers have successfully manufactured bilayer/multilayer 2D materials with tunable twist angle with the advancement of 2D materials preparation technologies in recent years [44]. A recently reported water-assisted transfer approach, in particular, allows for the clean transfer of tBLG [45]. The fabrication steps are as follows: i. Mechanically exfoliate the monolayer graphene on the patterned SiO_2/Si substrate; ii. Use the PDMS and water droplet to transfer monolayer graphene on top of the other; iii. Control the twist angle by rotation stage; and iv. Lift the PDMS film and characterize the tBLG. Traditional characterization methods such as spherical aberration electron microscopy (AC-TEM) and scanning tunneling electron microscopy (STM) can directly collect atomic lattice deformation information, but characterizing the strained moiré

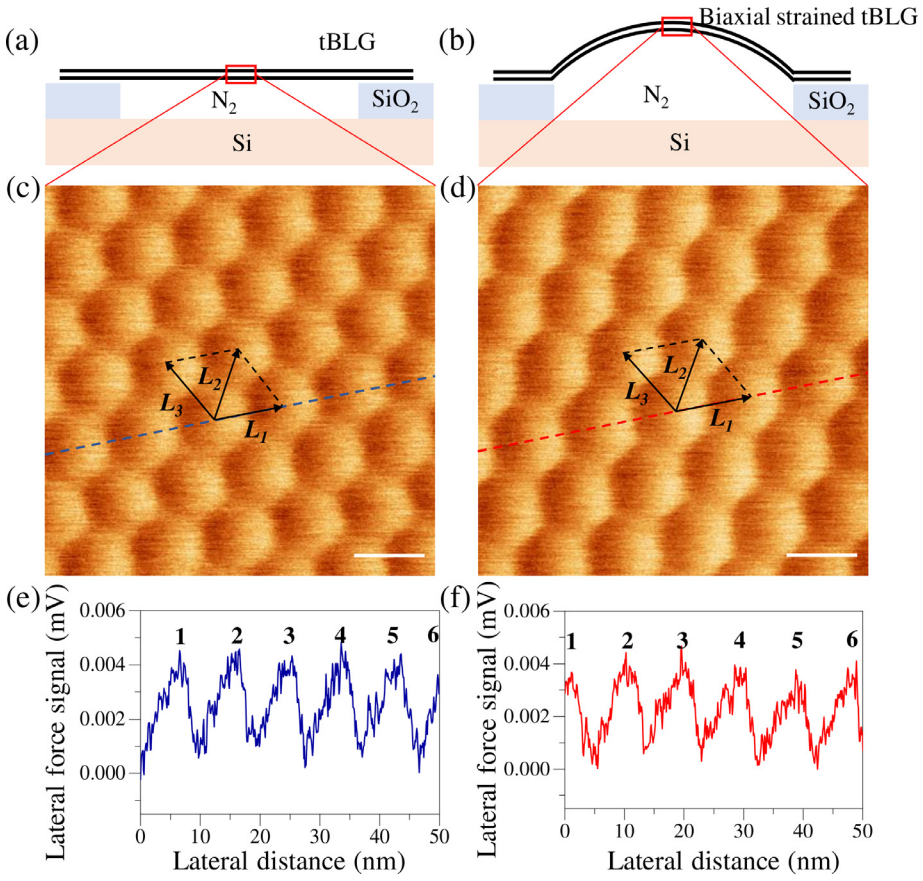

Fig. 4. Schematics of microbubble device of suspended tBLG: (a) before the nitrogen loading and (b) after the nitrogen loading. Lateral force images of moiré pattern of tBLG before (c) and after loading (d), where the black arrows denote the vectors of moiré pattern. Line-scanning results of moiré patterns before (e) and after loading (f), that along the dashed lines in (c) and (d), respectively. Scale bars: (c), (d) 10 nm.

pattern in-situ remains difficult. In this study, we employed AFM to generate atomic resolution images and moiré pattern images using the lateral force signal [45]. Flexible PDMS film would generate local residual strain in tBLG throughout the transfer process of tBLG [46], as shown in Fig. 3(a-c). To evaluate the residual strain of tBLG, since the residual strain introduced during the transfer process is random, we start by calculate the initial twist angle using the regular hexagonal moiré pattern as a reference point. Fig. 3(d-f) illustrate the lateral force picture and diffraction pattern of strain-free tBLG. The lengths of the moiré pattern in Fig. 3(d) are 23.5 nm, 23.4 nm, and 23.5 nm, respectively, which indicates the twist angle is ~0.6°. Fig. 3(d) and (e) depict asymmetric moiré and diffraction patterns induced by residual strain. We initially measure three lengths of moiré pattern in three directions to estimate the value and direction of the residual strain. By introducing three experimentally measured lengths of moiré pattern L_i^{exp}, a system of equations involving three unknowns (ϵ_1, ϵ_2, α) can be written as,

$$L_i^{exp} = L_i = \frac{4\pi}{\sqrt{3}|\boldsymbol{m}_i|}, i = 1, 2, 3 \tag{12}$$

We can answer Eq. (12) numerically because the twist angle is fixed in the experiment setup. The lengths of moiré pattern in Fig. 3(g) are measured to be 25.9 nm, 27.5 nm, 22.4 nm. Then ϵ_1, ϵ_2, α are solved to be ~0.31%, ~0.01%, ~13°, respectively. The local residual strain field of tBLG [Fig. 3(g)] is depicted in Fig. 3(i), with black arrows representing strain directions.

1.3. Characterization of local strain induced by microbubble experiment

Furthermore, using the microbubble approach, we characterize the change in moiré pattern when biaxial stretch strain is given to both the top and bottom layer of the suspended tBLG. In the microbubble experiment, suspended tBLG samples on patterned SiO_2/Si substrate were placed in an autoclave, and nitrogen was incrementally added to the autoclave using a booster pump. After a week of loading pressure, nitrogen progressively leaks into the hole through the interface between graphene and SiO_2. The pressure in the hole is higher than atmospheric pressure once the tBLG sample is removed from the autoclave, causing the tBLG to puff out and create a hemispherical bubble where the center of tBLG bubble is biaxially stretched. The detailed microbubble experimental methods can be found in prior work [47]. The schematics of the tBLG microbubble device are shown in Fig. 4(a) and (b). By using the nitrogen-loaded microbubble technique [48], we can apply the biaxial strain on the tBLG, and the strains in the central region of tBLG bubble can be determined by the ratio of height and radius of microbubble [49]. The moiré patterns (lateral force signal) of tBLG are shown in Fig. 4(c) and (d) before and after loading, with the lengths of the moiré pattern increasing as the strain rises. The average length of the unstrained moiré pattern is 9.40 nm, which suggests a twist angle of 1.5°, as shown in Fig. 4(e). The length of the moiré pattern is 9.43 nm, as seen in Fig. 4(f). Eq. (11) could therefore be used to compute the strain of the graphene lattice as ~0.32%. Furthermore, the ratio of microbubble height to radius is 0.067, resulting in biaxial tensile strain (~0.31%) in the center of tBLG bubble [49]. We may find that the relative error measured by the moiré method is roughly 3% by comparing the theoretical strain induced by microbubble experiment with the strain values obtained by our moiré method.

Given the fact that AFM spatial resolution and thermal drift are the main sources of error in this experiment, the precision of strain measured by moiré pattern differs with the varied initial twist angles. Since the residual strain we evaluated was randomly introduced by transfer process, the residual strain is obtained in this work by comparing with the reference regular hexagonal moiré pattern. Therefore, the current results are only relative values, and the measurement error of residual strain cannot be given.

2. Conclusion

We prepare the suspended tBLG and use the lengths of moiré pattern to evaluate the local strain fields. The mathematical model of graphene moiré pattern with strain is established through the examination of reciprocal vectors. We analyze the local residual strain of tBLG induced by transfer process and characterize the biaxial strain of tBLG applied by the microbubble experiment. The experimental results further highlight the feasibility of our strain analysis method.

Declaration of Competing Interest

The authors declare that there are no conflicts of interest related to this article.

Acknowledgements

This work is jointly supported by the National Natural Science Foundation of China (Grant Nos. 11890682, 11832010, and 21721002), the Strategic Priority Research Program of Chinese Academy of Sciences (CAS) under the Grant No. XDB30201000). We thank Dr. Guorui Wang, Dr. Zhaohe Dai and Dr. Yinbo Zhu for their fruitful suggestions for this work.

References

[1] Cao Y, et al. Correlated insulator behavior at half-filling in magic-angle graphene superlattices. Nature 2018;556(7699):80–4.
[2] Cao Y, Fatemi V, Fang S, Watanabe K, Taniguchi T, Kaxiras E, Jarillo-Herrero P. Unconventional superconductivity in magic-angle graphene superlattices. Nature 2018;556(7699):43–50.
[3] Li H, Wang J, Gao S, Chen Q, Peng L, Liu K, Wei X. Superlubricity between MoS_2 monolayers. Adv Mater 2017;29(27):1701474.
[4] Sinclair RC, Suter JL, Coveney PV. Graphene–graphene interactions: friction, superlubricity, and exfoliation. Adv Mater 2018;30(13):1705791.
[5] Koren E, Duerig U. Superlubricity in quasicrystalline twisted bilayer graphene. Phy Rev B 2016;93(20):201404.
[6] Kazmierczak NP, et al. Strain fields in twisted bilayer graphene. Nat Mater 2021;20(7):956–63.
[7] Kerelsky A, et al. Maximized electron interactions at the magic angle in twisted bilayer graphene. Nature 2019;572(7767):95–100.
[8] Yan W, et al. Strain and curvature induced evolution of electronic band structures in twisted graphene bilayer. Nat Commun 2013;4(1):1–7.
[9] Dai Z, Liu L, Zhang Z. Strain engineering of 2D materials: issues and opportunities at the interface. Adv Mater 2019;31(45):1805417.
[10] Oster G, Nishijima Y. Moiré patterns. Sci Am 1963;208:54–63.
[11] Sciammarella CA. The moiré method—a review. Exp Mech 1982;22(11):418–33.
[12] Dai F, Wang Z. Geometric micron-moiré. Opt Lasers Eng 1999;31(3):191–8.
[13] Theocaris PS. Chapter 2 - Moiré patterns formed by line gratings. In: Theocaris PS, editor. Moiré fringes in strain analysis. Pergamon; 1969. p. 19–111.
[14] Sciammarella C, Durelli A. Moiré fringes as a means of analyzing strains. J Eng Mech Div 1961;87(1):55–74.
[15] Ri S, Fujigaki M, Morimoto Y. Sampling moiré method for accurate small deformation distribution measurement. Exp Mech 2010;50(4):501–8.
[16] Li X, Xie H, Kang Y, Wu X. A brief review and prospect of experimental solid mechanics in China. Acta Mechanica Solida Sinica 2010;23(6):498–548.
[17] Kamal H, Völkel R, Alda J. Properties of moiré magnifiers. Opt Eng 1998;37(11):3007–14.
[18] Post D, Han B, Ifju PG. Moiré methods for engineering and science—moiré interferometry and shadow moiré. Photomechanics 2000;77:151–96.
[19] Wang N, Jiang W, Zhang Y. Moiré-based sub-nano misalignment sensing via deep learning for lithography. Opt Lasers Eng 2021;143(8):106620.
[20] Chiang F-P. Moiré methods of strain analysis. Exp Mech 1979;19(8):290–308.
[21] Asundi A. Moiré Interferometry for deformation measurement. Opt Lasers Eng 1989;11(4):281–92.
[22] Xie H, Shang H, Xue Q, Jia J, Dai F. Defects analysis of Al/Si artificial nanocluster with moiré fringes. Opt Laser Eng 2005;43(10):1071–80.
[23] Huguenin J, dos Santos BC, Dos Santos P, Khoury A. Topological defects in moiré fringes with spiral zone plates. JOSA A 2003;20(10):1883–9.
[24] Wang K, Qu C, Wang J, Ouyang W, Ma M, Zheng Q. Strain engineering modulates graphene interlayer friction by moiré pattern evolution. ACS Appl Mater Interfaces 2019;11(39):36169–76.
[25] Liu Z, Xie H, Fang D, Shang H, Dai F. A novel nano-moiré method with scanning tunneling microscope (STM). J Mat Proc Tech 2004;148(1):77–82.
[26] Li G, Luican A, Andrei EY. Scanning tunneling spectroscopy of graphene on graphite. Phys Rev Lett 2009;102(17):176804.
[27] McGilly LJ, et al. Visualization of moiré superlattices. Nat Nanotechnol 2020;15(7):580–4.
[28] Woods CR, et al. Commensurate–incommensurate transition in graphene on hexagonal boron nitride. Nat Phys 2014;10:451–6.
[29] Li G, Luican A, dos Santos J M B L, Castro Neto AH, Reina A, Kong J, et al. Observation of Van Hove singularities in twisted graphene layers. Nat Phys 2010;6:109–13.
[30] Warner JH, Rümmeli MH, Gemming T, Büchner B, Briggs GAD. Direct imaging of rotational stacking faults in few layer graphene. Nano Lett 2009;9(1):102–6.
[31] He F, Zhou Y, Ye Z, Cho S-H, Jeong J, Meng X, Wang Y. Moiré patterns in 2D materials: a review. ACS Nano 2021;15(4):5944–58.
[32] Lu C, Lin Y, Liu Z, Yeh C, Suenaga K, Chiu P. Twisting bilayer graphene superlattices. ACS Nano 2013;7(3):2587–94.
[33] Zhang K, Tadmor EB. Structural and electron diffraction scaling of twisted graphene bilayers. J Mech Phys Solids 2018;112:225–38.
[34] Jiang Y, Mao J, Duan J, Lai X, Watanabe K, Taniguchi T, Andrei EY. Visualizing strain-induced pseudomagnetic fields in graphene through an hBN magnifying glass. Nano Lett 2017;17(5):2839–43.
[35] Andrei EY, MacDonald AH. Graphene bilayers with a twist. Nat Mater 2020;19(12):1265–75.
[36] Miller DL, Kubista KD, Rutter GM, Ruan M, de Heer WA, First PN, Stroscio JA. Structural analysis of multilayer graphene via atomic moiré interferometry. Phys Rev B 2010;81(12):125427.
[37] Wang Q, Kishimoto S, Yamauchi Y. Three-directional structural characterization of hexagonal packed nanoparticles by hexagonal digital moiré method. Opt Lett 2012;37(4):548–50.
[38] Cosma Diana A, Wallbank John R, Cheianov Vadim, Falko Vladimir. Moiré pattern as a magnifying glass for strain and dislocations in Van der Waals heterostructures. Faraday Discuss 2014;173:137–43.
[39] Wang Z, Wang Y, Yin J, Tóvári E, Yang Y, Lin L, et al. Composite super-moiré lattices in double-aligned graphene heterostructures. Sci Adv 2019;5:eaay8897.
[40] MacDonald AH, Bistritzer R. Graphene moiré mystery solved? Nature 2011;474(7352):453–4.
[41] Dai S, Xiang Y, Srolovitz DJ. Twisted bilayer graphene: moiré with a twist. Nano Lett 2016;16(9):5923–7.
[42] Huder L, et al. Electronic spectrum of twisted graphene layers under heterostrain. Phys Rev Lett 2018;120(15):156405.
[43] Qiao J, Yin L, He L. Twisted graphene bilayer around the first magic angle engineered by heterostrain. Phys Rev B 2018;98(23):235402.
[44] Frisenda R, Navarro-Moratalla E, Gant P, Perez De Lara D, Jarillo-Herrero P, Gorbachev RV, Castellanos-Gomez A. Recent progress in the assembly of nanodevices and Van der Waals heterostructures by deterministic placement of 2D materials. Chem Soc Rev 2018;47(1):53–68.
[45] Hou Y, et al. Preparation of twisted bilayer graphene via the wetting transfer method. ACS Appl Mater Interfaces 2020;12(36):40958–67.
[46] Sanchez DA, Dai Z, Wang P, Cantu-Chavez A, Brennan CJ, Huang R, Lu N. Mechanics of spontaneously formed nanoblisters trapped by transferred 2D crystals. Proc Natl Acad Sci 2018;115(31):7884–9.
[47] Wang G, Dai Z, Wang Y, Tan P, Liu L, Xu Z, Wei Y, Huang R, Zhang Z. Measuring interlayer shear stress in bilayer graphene. Phys Rev Lett 2017;119(3):036101.
[48] Zhang S, Hou Y, Li S, Liu L, Zhang Z, Feng X, et al. Tuning friction to a superlubric state via in-plane straining. Proc Natl Acad Sci 2005;116(49):24452–6.
[49] Dai Z, et al. Interface-governed deformation of nanobubbles and nanotents formed by two-dimensional materials. Phys Rev Lett 2018;121(26):266101.